




**Twistons in graphene nanoribbons on a substrate**A. V. Savin <sup>1,2</sup>, E. A. Korznikova <sup>3,4</sup> and S. V. Dmitriev <sup>3,4</sup><sup>1</sup>*N. N. Semenov Federal Research Center for Chemical Physics, Russian Academy of Sciences (FRCCP RAS), Moscow 119991, Russia*<sup>2</sup>*Plekhanov Russian University of Economics, Moscow 117997, Russia*<sup>3</sup>*Institute for Molecule and Crystal Physics, Ufa Federal Research Centre of Russian Academy of Sciences, Ufa 450075, Russia*<sup>4</sup>*Ufa State Petroleum Technological University, 1 Kosmonavtov Street, Ufa 450064, Russia*

(Received 12 July 2020; revised 20 September 2020; accepted 23 October 2020; published 30 December 2020)

Twisted nanoribbons from two-dimensional materials possess many unusual properties tunable by changing the twist angle, for example, electro- and thermal conductivity, chemical properties, and stability against buckling. New interesting phenomena can be observed when a twisted nanoribbon interacts with a substrate. Here we report the results of a classical molecular dynamics study of a graphene nanoribbon twisted about its long axis and interacting with a graphite substrate. Van der Waals interactions with the substrate lead to localization of twisting and the formation of topological solitons called *twistons*. The topological charge of a twiston obtained with the twist angle  $\beta$  multiple of  $\pi$  can be defined as  $q = \beta/\pi$ ; it can be positive or negative. Twistons can move along the nanoribbon with very little radiation in the form of small-amplitude phonons. Scenarios of twiston collisions are described depending on their topological charge and on the nanoribbon width. In narrow nanoribbons twistons collide practically elastically, preserving their profiles and speeds after the collision, and inelasticity of collisions increases with increasing nanoribbon width. Our results contribute to an understanding of the behavior of two-dimensional material nanoribbons on a substrate.

DOI: [10.1103/PhysRevB.102.245432](https://doi.org/10.1103/PhysRevB.102.245432)**I. INTRODUCTION**

Nanostructures composed of  $sp^2$  carbon, such as graphene and carbon nanotubes, demonstrate a very high thermal conductivity [1,2], outstanding mechanical properties including record stiffness and tensile strength under tension [3,4], optical conductance [5], high electron mobility [6], and biological compatibility [7].

Two-dimensional (2D) nanomaterials are easy to bend or crumple, and they can be stabilized in such deformed states by van der Waals forces. Secondary 3D structures of graphene are presented by nanoscrolls or folds [8–12], windings around carbon nanotubes [13,14], ripples and wrinkles [15–18], crumpled graphene [19,20], kirigami and origami structures obtained by cutting or folding [21–24], carbon nanotube bundles [25–28], and others. Graphene can also be twisted by applying external forces or spontaneously [29–36]. Graft polymers have the form of a coil [37]. Actually, wrinkling, folding, rolling, and twisting are common to any thin-sheet material [38–41].

The prediction of materials' behavior and properties in the presence of twist deformation is an issue of particular importance, e.g., for design of reliable materials for flexible electronics [42–44]. Note that in those works and in the present study, graphene nanoribbons are twisted about the long axis and here we do not discuss twisted bilayer graphene [45].

The effect of twisting on the mechanical properties of nanoribbons has been considered in the works [46–48]. The relationship between the shear stress and the twist angle

was obtained for a graphene nanoribbon encapsulated in a single-walled carbon nanotube [49]. Nanoribbon twisting increases the area moment of inertia, which improves resistance to lateral buckling under axial compression [47,48]. Structural transition in helicoidal nanosprings has been revealed and explained by van der Waals interlayer interactions [50]. Electronic properties of twisted graphene, silicene, and black phosphorus nanoribbons have been analyzed in Refs. [51–58]. The twisting of nanoribbons results in nonhomogeneous deformation across the nanoribbon, which leads to formation of spatially localized phonon states [36]. The thermal conductivity of twisted nanoribbons was studied in Refs. [48,59–62]. According to the study [48], the thermal conductivity of twisted graphene nanoribbon as the function of the twist angle first increases quadratically, then starts to decrease after reaching a maximum. This is explained by the competition of two factors: for small twist angles tensile strain is induced along the nanoribbon edges, which enhances the contribution to thermal conductivity from ZA phonons. For larger twist angles, tensile strain reduces the rigidity of valence bonds, which slows down phonon group velocity and reduces thermal conductivity [48]. Decrease of thermal conductivity was observed for folded [8], wrinkled [63], coiled [64], and twisted [65] graphene. Kirigami graphene can demonstrate a considerably enhanced thermal conductivity [66].

2D materials can support propagation of solitary waves, for example, shock waves [67], wrinklons [16], ripplocations [68–72], and discrete breathers [73–75].

Our aim here is to study the interaction of twisted graphene nanoribbons with a graphite substrate and the emergence

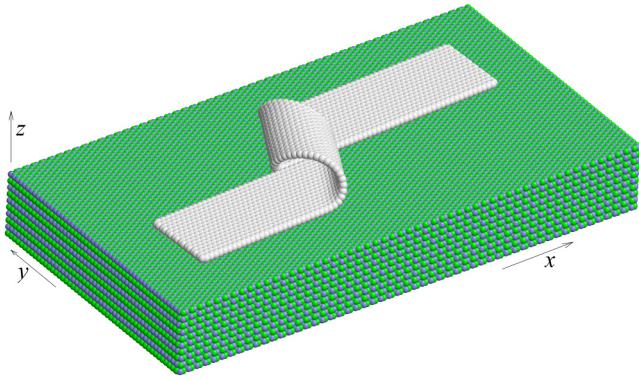


FIG. 1. The stationary state of a  $2\pi$  twiston in a graphene nanoribbon of  $N = 100$  transverse cells (length  $L_x = 24.31$  nm) and  $K = 32$  (width  $L_y = 3.26$  nm) on the *h*-BN substrate.

of localized states, here called twistons. Note that the term *twiston* was used earlier for long-wave phonon torsion vibrations of carbon nanotubes [76,77]. However, in the present study, this term is used for topological solitons that appear in twisted nanoribbons interacting with a substrate; see Fig. 1.

Suppose the nanoribbon is twisted by the angle  $\beta$  multiple of  $\pi$ . If the nanoribbon interacts with a substrate, the twisted region will be localized and a twiston with the topological charge  $q = \beta/\pi$  will be formed.

We describe the computational model in Sec. II and report properties of equilibrium twistons in Sec. III. Twiston dynamics are analyzed in Sec. IV, twiston collisions are investigated in Sec. V, and Sec. VI concludes our work.

## II. MODEL

Our simulations are performed with the use of classical molecular dynamics based on the interatomic potentials developed in Ref. [78].

A rectangular graphene nanoribbon with a zigzag longitudinal edge consisting of  $N \times K$  carbon atoms is considered; see Fig. 2(a). Here  $N$  is the number of transverse translational cells separated by the vertical dotted lines numbered by index  $n$ ,  $K$  is the even number of atoms in the cell indexed by  $k$ ,  $r_0 = 1.418$  Å is equilibrium valence bond length, and the longitudinal period of the nanoribbon is  $a = \sqrt{3}r_0 = 2.456$  Å. Nanoribbon length is  $L_x = (N - 1)a$  and width is  $L_y = (3K/4 - 1)r_0$ . Carbon atoms have a mass  $M_0 = 12m_p$ , where  $m_p = 1.6601 \times 10^{-27}$  kg is the proton mass. It is assumed that the atoms at the nanoribbon edges are chemically modified by hydrogen atoms, which is taken into account by setting the mass of the edge atoms  $M_1 = 13m_p$ .

The surface of crystalline graphite is used as a flat substrate for the nanoribbon. The properties of graphite and other substrates are discussed below.

The Hamiltonian of the system includes four terms,

$$H = T + P + V + Z, \quad (1)$$

where  $T$  is the kinetic energy of atoms,  $P$  is the potential energy of valence C-C interactions in the nanoribbon,  $V$  is the energy of van der Waals interactions in the nanoribbon,

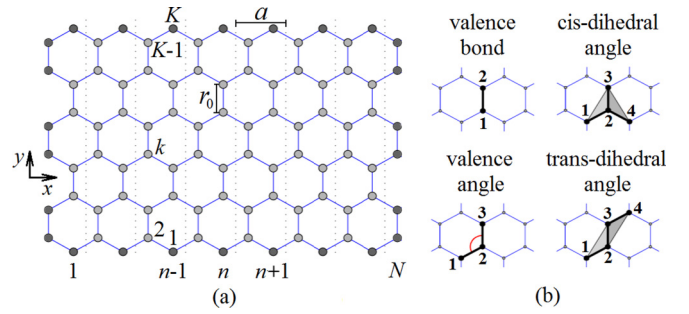


FIG. 2. (a) Graphene nanoribbon in the  $x, y$  plane with the  $x$  axis ( $y$  axis) oriented along the zigzag (armchair) direction;  $r_0 = 1.418$  Å is equilibrium valence bond length. The longitudinal period of the nanoribbon is  $a = \sqrt{3}r_0$ . Transverse translational cells separated by the vertical dotted lines are numbered by the index  $n = 1, 2, \dots, N$  and the atoms in each cell are indexed by  $k = 1, 2, \dots, K$  ( $K$  is even). Nanoribbon length is  $L_x = (N - 1)a$  and width is  $L_y = (3K/4 - 1)r_0$ . The edge atoms shown in dark gray are chemically modified by hydrogen atoms. (b) Interatomic interactions described by the potential Eq. (4) including the energy of valence bonds, valence angles, and *cis*- and *trans*-dihedral angles.

and  $Z$  is the potential energy of the van der Waals interactions between the nanoribbon and the substrate.

Let

$$\mathbf{u}_{n,k}(t) = (x_{n,k}(t), y_{n,k}(t), z_{n,k}(t)) \quad (2)$$

be the radius vector describing the position of an atom with the indices  $n, k$  at the time  $t$ .

Kinetic energy is calculated according to the expression

$$T = \frac{1}{2} \sum_{n=1}^N \sum_{k=1}^K M_{n,k} (\dot{\mathbf{u}}_{n,k}, \dot{\mathbf{u}}_{n,k}), \quad (3)$$

where the mass of the carbon atom  $M_{n,k} = M_1$  for the edge atoms and  $M_{n,k} = M_0$  otherwise; the overdot denotes differentiation with respect to time, so that  $\dot{\mathbf{u}}_{n,k}$  is the atom velocity vector and the round brackets represent the inner product.

The valence part of the potential depends on variations in bond lengths, bond angles, and *cis*- and *trans*-dihedral angles between the planes formed by four neighboring carbon atoms [see Fig. 2(b)] and it can be written in the form

$$P = \sum_{\Omega_1} U_1 + \sum_{\Omega_2} U_2 + \sum_{\Omega_3} U_3 + \sum_{\Omega_4} U_4. \quad (4)$$

Here summation over  $\Omega_i$ , with  $i = 1, 2, 3, 4$ , means the summation over all valence bonds, valence angles, and *cis*- and *trans*-dihedral angles of the nanoribbon, respectively [79]. Valence bonds are described by the Morse potential

$$U_1(\mathbf{u}_1, \mathbf{u}_2) = \epsilon_1 \{ \exp[-\alpha_0(r - r_0)] - 1 \}^2, \quad r = |\mathbf{u}_2 - \mathbf{u}_1|, \quad (5)$$

where  $\epsilon_1 = 4.9632$  eV is the energy of the C-C valence bond and bond stiffness is  $\alpha_0 = 1.7889$  Å<sup>-1</sup>. For the valence angle the potential reads

$$U_2(\mathbf{u}_1, \mathbf{u}_2, \mathbf{u}_3) = \epsilon_2 (\cos \varphi - \cos \varphi_0)^2, \quad (6)$$

$$\cos \varphi = (\mathbf{u}_3 - \mathbf{u}_2, \mathbf{u}_1 - \mathbf{u}_2) / (|\mathbf{u}_3 - \mathbf{u}_2| \cdot |\mathbf{u}_2 - \mathbf{u}_1|), \quad (7)$$

where  $\epsilon_2 = 1.3143$  eV, and the equilibrium value of the angle is  $\varphi_0 = 2\pi/3$ . The numerator of Eq. (7) is the inner product of vectors  $\mathbf{u}_3 - \mathbf{u}_2$  and  $\mathbf{u}_1 - \mathbf{u}_2$ , and the denominator is the product of their moduli.

The potential for the *cis*- and *trans*-dihedral angles is

$$U_i(\mathbf{u}_1, \mathbf{u}_2, \mathbf{u}_3, \mathbf{u}_4) = \epsilon_i(\cos \phi), \quad (8)$$

$$\cos \phi = (\mathbf{v}_1, \mathbf{v}_2)/(|\mathbf{v}_1| \cdot |\mathbf{v}_2|), \quad (9)$$

$$\mathbf{v}_1 = (\mathbf{u}_2 - \mathbf{u}_1) \times (\mathbf{u}_3 - \mathbf{u}_2), \quad (10)$$

$$\mathbf{v}_2 = (\mathbf{u}_3 - \mathbf{u}_2) \times (\mathbf{u}_3 - \mathbf{u}_4), \quad (11)$$

where  $\epsilon_3 = \epsilon_4 = 0.499$  eV and the equilibrium value of the dihedral angle is  $\pi$ .

Nonvalence interactions of the carbon atoms of the nanoribbon are described by the (6,12) Lennard-Jones potential [80]

$$U_0(r) = \epsilon_c \{ [(r_c/r)^6 - 1]^2 - 1 \}, \quad (12)$$

where  $\epsilon_c = 0.002757$  eV,  $r_c = 3.807$  Å.

The energy of van der Waals interactions in the nanoribbon in Eq. (1) is

$$V = \sum_{\Omega_0} U_0, \quad (13)$$

where summation over  $\Omega_0$  means the summation over all pairs of atoms which do not interact via any of the valence bonds  $U_i$ ,  $i = 1, 2, 3, 4$ .

The van der Waals interactions of the carbon atoms of the nanoribbon with a substrate in Eq. (1) are described by the Lennard-Jones potential ( $m, l$ ):

$$Z = \sum_{n=1}^N \sum_{k=1}^K W(z_{n,k}),$$

$$W(z) = \epsilon_z [m(z_0/z)^l - l(z_0/z)^m]/(l - m), \quad (14)$$

where  $z_{n,k}$  is the distance from the nanoribbon carbon atom to the outer surface of the substrate, which is the plane  $z = 0$ .  $W(z)$  in Eq. (14) is the interaction energy of a carbon atom of the nanoribbon as a function of the distance to the substrate. This energy was found numerically for different substrates [68,81]. It was shown that the energy  $W(z)$  can be described with high accuracy by the ( $m, l$ ) Lennard-Jones potential, where the exponents satisfy  $l > m$ . The potential  $W(z)$  has a minimum at  $z = z_0$  with  $W(z_0) = -\epsilon_z$ . This means that the binding energy of a carbon atom with the substrate is  $\epsilon_z$  and  $z_0$  is the equilibrium distance from the plane of the substrate surface.

Parameters of the potential  $W(z)$  for different substrates are as follows [68,81]. For the ice crystal surface  $I_h$ , the interaction energy is  $\epsilon_z = 0.029$  eV, the equilibrium distance is  $z_0 = 3.005$  Å, and the exponents are  $l = 10$ ,  $m = 3.5$ . For the surface of the  $\alpha$ -graphite crystal,  $\epsilon_z = 0.0518$  eV,  $z_0 = 3.37$  Å,  $l = 10$ ,  $m = 3.75$ . For the surface of the hexagonal boron nitride crystal (*h*-BN),  $\epsilon_z = 0.0903$  eV,  $z_0 = 3.46$  Å,  $l = 10$ ,  $m = 3.75$ .

Further information on the development of the interatomic potentials used in this study can be found in the works [78,82].

The initial conditions are described below for each specific problem.

### III. EQUILIBRIUM STATES OF TWISTED NANORIBBONS ON THE SUBSTRATE

To find the equilibrium state of a nanoribbon, the potential energy minimization problem,

$$E = P + V + Z \rightarrow \min : \{ \mathbf{u}_{n,k} \}_{n=1, k=1}^{N, K}, \quad (15)$$

is solved numerically using the conjugate gradient method.

Initial configurations are created as follows. The nanoribbon is divided into three parts  $1 \leq n \leq N_1$ ,  $N_1 < n < N_2$ ,  $N_2 \leq n \leq N$  and the second (middle) part turns in vacuum into a helicoid with a twist angle multiple of  $\pi$ . The first and third parts remain flat and parallel to the substrate, which is parallel to the  $x, y$  plane. Then, the following problem of energy minimization is solved numerically,

$$P + V + \sum_{n=1}^N \delta_n \sum_{k=1}^K W(z_{n,k}) \rightarrow \min :$$

$$\delta_n = 1 \text{ for } n \leq N_1, n \geq N_2; \delta_n = 0 \text{ for } N_1 < n < N_2, \quad (16)$$

where the interaction of the middle part of the nanoribbon with the substrate is switched off. Thus, the stationary state of the twisted nanoribbon was obtained, the ends of which ( $n \leq N_1$ ,  $n \geq N_2$ ) are in contact with the flat substrate, and the central (twisted) part ( $N_1 < n < N_2$ ) is in a suspended state. The solution to problem Eq. (15) was obtained from the solution to problem Eq. (16) in the limit  $N_1 \rightarrow N/2$ ,  $N_2 \rightarrow N/2 + 1$ , i.e., when the length of the suspended part of the nanoribbon vanishes.

In order to characterize the geometry and energy of twistons we consider the total energy per atom in the  $n$ th transverse cell of the nanoribbon,

$$E_n = T_n + P_n + V_n + Z_n, \quad (17)$$

where  $T_n$ ,  $P_n$ ,  $V_n$ , and  $Z_n$  are the kinetic energy, valence and van der Waals potential energy of the nanoribbon, and energy of interactions between the nanoribbon and the substrate per atom in the  $n$ th transverse cell of the nanoribbon, respectively. These energies are calculated using the expressions given above for  $T$ ,  $P$ ,  $V$ , and  $Z$  performing summations over the  $n$ th transverse cell.

We define the energy density distribution along the nanoribbon as

$$p_n = \frac{E_n - E_0}{\sum_{n=1}^N (E_n - E_0)}, \quad (18)$$

where  $E_0$  is the energy level of the system in the ground state and the numerator gives the deviation of the total energy of the transverse cell from the ground level. Then the  $x$  coordinate of the center of the twiston can be found as the center of gravity of  $p_n$ ,

$$\bar{x} = a\bar{n} = a \sum_{n=1}^N n p_n. \quad (19)$$

TABLE I. Dependence of the normalized energy  $E/K$ , dimensionless diameter  $D/a$ , and vertical amplitude  $A$  for the  $2\pi$  twiston on the number of atoms in the transverse cell of the nanoribbon  $K$  (on the nanoribbon width) for a nanoribbon lying on a flat crystal surface of ice  $I_h$ ,  $\alpha$ -graphite, and  $h$ -BN (energies are in eV, amplitudes in nm).

		$K$			
		8	16	32	64
Ice $I_h$	$E/K$	1.0778	1.2619	1.4566	1.8593
	$D/a$	11.16	13.82	18.90	31.35
	$A$	1.600	1.876	2.214	2.829
$\alpha$ -graphite	$E/K$	1.4445	1.7071	2.0511	2.8081
	$D/a$	10.68	12.81	17.67	29.82
	$A$	1.437	1.631	2.924	2.379
$h$ -BN	$E/K$	1.8876	2.3008	2.9337	4.2195
	$D/a$	8.01	10.90	16.50	28.17
	$A$	1.051	1.305	1.652	2.001

The diameter (width) of the twiston can be calculated as

$$D = a \left\{ 1 + 2 \left[ \sum_{n=1}^N (n - \bar{n})^2 p_n \right]^{1/2} \right\}. \quad (20)$$

The twiston profile is also characterized by the maximal distance of the atoms in  $n$ th transverse cell from the substrate,

$$A_n = \max_{1 \leq k \leq K} z_{n,k}. \quad (21)$$

The twiston vertical amplitude is

$$A = \max_{1 \leq n \leq N} A_n. \quad (22)$$

First we discuss the effect of the substrate on the equilibrium structure of the  $2\pi$  twiston and then the main results are presented for the  $\alpha$ -graphite substrate.

### A. Effect of the substrate

The result of relaxation for a nanoribbon of length  $L_x = 24.31$  nm ( $N = 100$ ) and width  $L_y = 3.26$  nm ( $K = 32$ ), lying on the  $h$ -BN substrate, is shown in Fig. 1 for twist angle  $2\pi$ . The  $2\pi$ -twiston is formed in the middle of the nanoribbon.

We calculate the normalized potential energy of the twiston,  $E/K$ , the dimensionless diameter,  $D/a$ , and the twiston amplitude  $A$ . These parameters are collected in Table I for the three different substrates and for four different values of  $K$ , which define the nanoribbon width.

Analyzing the data presented in Table I, one can conclude that, for any substrate, twiston energy, diameter, and amplitude grow with increasing nanoribbon width (with  $K$ ). Comparison of the results for different substrates reveals that the twiston energy is minimal for ice, maximal for  $h$ -BN, and has intermediate value for graphite. This correlates with the strength of interaction of graphene nanoribbon with the substrate,  $\epsilon_z$ , which is minimal for ice and maximal for  $h$ -BN. On the other hand, twiston diameter and amplitude decrease with increasing  $\epsilon_z$ , being maximal for ice and minimal for  $h$ -BN.

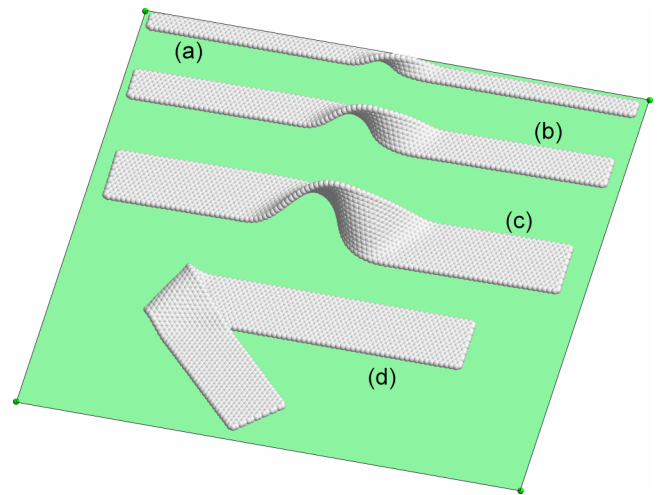


FIG. 3. The stationary states of  $\pi$  twistons in a nanoribbon of  $N = 100$  transverse cells (length  $L_x = 24.31$  nm) and different widths: (a)  $K = 8$  ( $L_y = 0.7090$  nm), (b)  $K = 16$  ( $L_y = 1.560$  nm), and (c)  $K = 28$  ( $L_y = 2.836$  nm). Energy of twistons is  $E = 6.103$ ,  $22.533$ , and  $60.597$  eV. Twiston width is  $D = 2.149$ ,  $3.483$ , and  $4.998$  nm. (d) Tilted fold topologically equivalent to the twiston in (c) formed from the twiston as the result of relaxation in the presence of small perturbations; energy of the fold is  $39.28$  eV. A flat graphite substrate is shown in green (gray).

### B. Graphite substrate

In the rest of this work  $\alpha$ -graphite is taken as the substrate.

The result of relaxation for nanoribbons of length  $L_x = 24.31$  nm ( $N = 100$ ) and different widths is shown in Fig. 3 and Fig. 4 for twist angles equal to  $\pi$  and  $2\pi$ , respectively.

In Fig. 3, the nanoribbon width is (a)  $K = 8$  ( $L_y = 0.709$  nm), (b)  $K = 16$  ( $L_y = 1.56$  nm), and (c)  $K = 28$  ( $L_y = 2.836$  nm). Static  $\pi$  twistons in (a) to (c) have energy  $E_\pi = 6.103$ ,

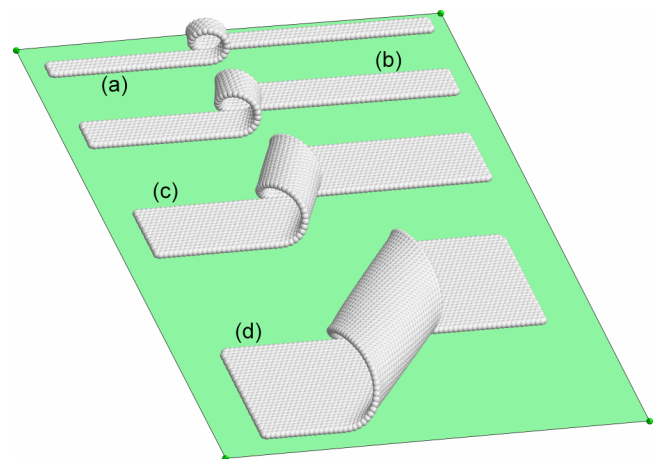


FIG. 4. The stationary states of  $2\pi$  twistons in a nanoribbon of  $N = 100$  transverse translational cells (length  $L_x = 24.31$  nm) and different widths: (a)  $K = 8$  ( $L_y = 0.709$  nm), (b)  $K = 16$  ( $L_y = 1.56$  nm), (c)  $K = 32$  ( $L_y = 3.261$  nm), and (d)  $K = 64$  ( $L_y = 6.665$  nm). Energy of twistons is  $E = 11.51$ ,  $27.19$ ,  $65.32$ , and  $179.0$  eV, respectively. Twiston width is  $D = 2.623$ ,  $3.146$ ,  $4.340$ , and  $7.324$  nm, respectively.



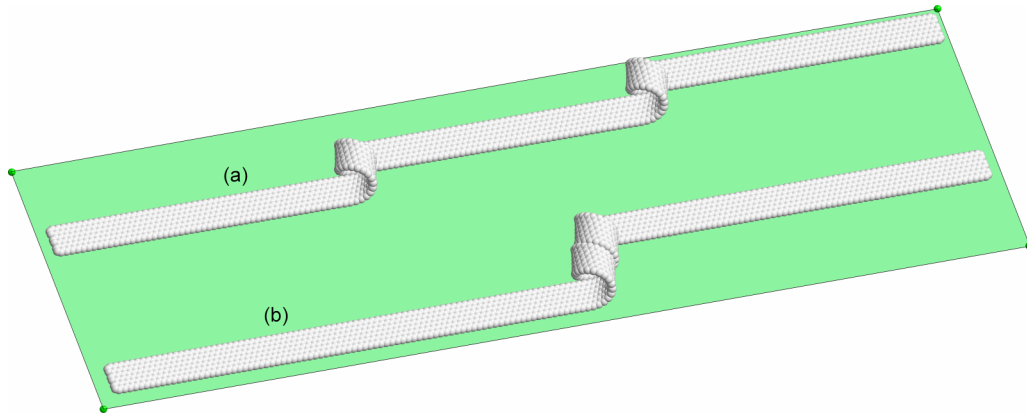


FIG. 5. The stationary states of (a) two isolated  $2\pi$  twistons (energy  $2E_{2\pi} = 38.236$  eV) and (b) the bound state of two  $2\pi$  twistons ( $E_{2\pi+2\pi} = 37.684$  eV) in a nanoribbon with length  $N = 200$ ,  $L_x = 48.87$  nm, and width  $K = 12$  ( $L_y = 1.134$  nm).

22.533, and 60.597 eV, respectively. Twistons in (a) to (c) have width  $D = 2.149$ , 3.483, and 4.998 nm, respectively. It turns out that the twistons in relatively narrow nanoribbons, e.g., in (a) and (b), are stable. The  $\pi$  twiston in (c) is metastable and after relaxation in presence of small perturbations it transforms into the topologically equivalent tilted fold shown in (d). The energy of the fold in (d) is  $E = 39.28$  eV which is about  $2/3$  of the twiston energy in (c).

In Fig. 4, the nanoribbon width is (a)  $K = 8$  ( $L_y = 0.709$  nm), (b)  $K = 16$  ( $L_y = 1.56$  nm), (c)  $K = 32$  ( $L_y = 3.261$  nm), and (d)  $K = 64$  ( $L_y = 6.665$  nm). The energy of static  $2\pi$  twistons in (a) to (d) is  $E_{2\pi} = 11.51$ , 27.19, 65.32, and 179.0 eV, respectively. The width of twistons in (a) to (d) is  $D = 2.623$ , 3.146, 4.34, and 7.324 nm, respectively. In all cases  $2\pi$  twistons are stable with respect to small perturbations.

Note that the  $2\pi$  twiston is topologically equivalent to two  $\pi$  twistons. Interestingly, the energy of a  $2\pi$  twiston is always smaller than the energy of two  $\pi$  twistons,  $E_{2\pi} < 2E_{\pi}$ . Thus, the formation of a bound state of two  $\pi$  twistons leads to a significant energy gain, especially for wide nanoribbons.

In Fig. 5, stationary states of (a) two separated  $2\pi$  twistons and (b) the bound state of two  $2\pi$  twistons are shown. In both cases the nanoribbon width is  $K = 12$  ( $L_y = 1.134$  nm), and length is  $N = 200$  ( $L_x = 48.87$  nm). The energies of the structures in (a) and (b) are  $2E_{2\pi} = 38.236$  and  $E_{2\pi+2\pi} = 37.684$  eV, respectively. The bound state has somewhat smaller energy meaning that the  $2\pi$  twistons attract each other even though their topological charge is the same. Actually the bound state can be regarded as a  $4\pi$  twiston (binding energy  $2E_{2\pi} - E_{2\pi+2\pi} = 0.552$  eV).

The structure of other stationary  $4\pi$  twistons is presented in Fig. 6 in nanoribbons of different widths: (a)  $K = 12$  ( $L_y = 1.134$  nm, twiston energy  $E_{4\pi} = 34.51$  eV), (b)  $K = 20$  ( $L_y = 1.985$  nm,  $E_{4\pi} = 66.43$  eV), and (c)  $K = 40$  ( $L_y = 4.112$  nm,  $E_{4\pi} = 161.9$  eV). The nanoribbon length here is  $N = 200$ ,  $L_x = 48.87$  nm. We note that the energy of the  $4\pi$  twiston in (a) is smaller than the energy of the bound state of two  $2\pi$  twistons shown in Fig. 5(b) ( $E_{4\pi} < E_{2\pi+2\pi}$ ). Twistons in Figs. 6(a) and 6(b) produce a tilt angle for the nanoribbon ends, while the high-symmetry twiston in Fig. 6(c) does not.

Figure 7 presents the effect of the nanoribbon width ( $K$ ) on (a) energy  $E$ , (b) width  $D$ , and (c) amplitude  $A$  of the  $\pi$  twistons [see Figs. 3(a)–3(c)],  $2\pi$  twistons [see Figs. 4(a)–4(d)], and topologically equivalent tilted fold [see Fig. 3(d)]. Note that the energy in (a) is normalized to the nanoribbon width  $K$ . Twiston width in (b) is normalized to the longitudinal period of the nanoribbon  $a$ .

In Fig. 7, curves 1, 4, and 7 give the results for the  $2\pi$  twiston; curves 2, 5, and 8 stand for the  $\pi$  twiston; and curves 3, 6, and 9 for the tilted fold. As can be seen from (a), the  $\pi$  twiston has the lowest energy in narrow nanoribbons ( $K < 7$ ) and for larger width the  $2\pi$  twiston has the lowest energy. The tilted fold has energy lower than the  $\pi$  twiston for  $K > 14$  meaning that in wide nanoribbons the  $\pi$  twiston is unstable and transforms into the tilted fold, as illustrated in Figs. 3(c) and 3(d). The driving force for this transformation is the increase in the number of van der Waals bonds. Curves in (b) increase monotonically for the  $\pi$  twiston (curve 4) and  $2\pi$  twiston (curve 5). On the other hand, the width of the tilted fold (curve 6) has a maximum at  $K = 34$  and decreases for

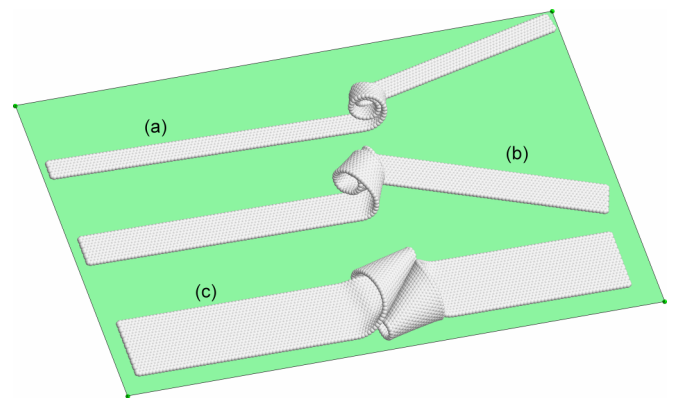


FIG. 6. The stationary states of  $4\pi$  twistons in nanoribbons of width (a)  $K = 12$  ( $L_y = 1.134$  nm, energy  $E_{4\pi} = 34.51$  eV), (b)  $K = 20$  ( $L_y = 1.985$  nm,  $E_{4\pi} = 66.43$  eV), and (c)  $K = 40$  ( $L_y = 4.112$  nm,  $E_{4\pi} = 161.9$  eV). Nanoribbon in all three cases has  $N = 200$  transverse cells and length  $L_x = 48.87$  nm.

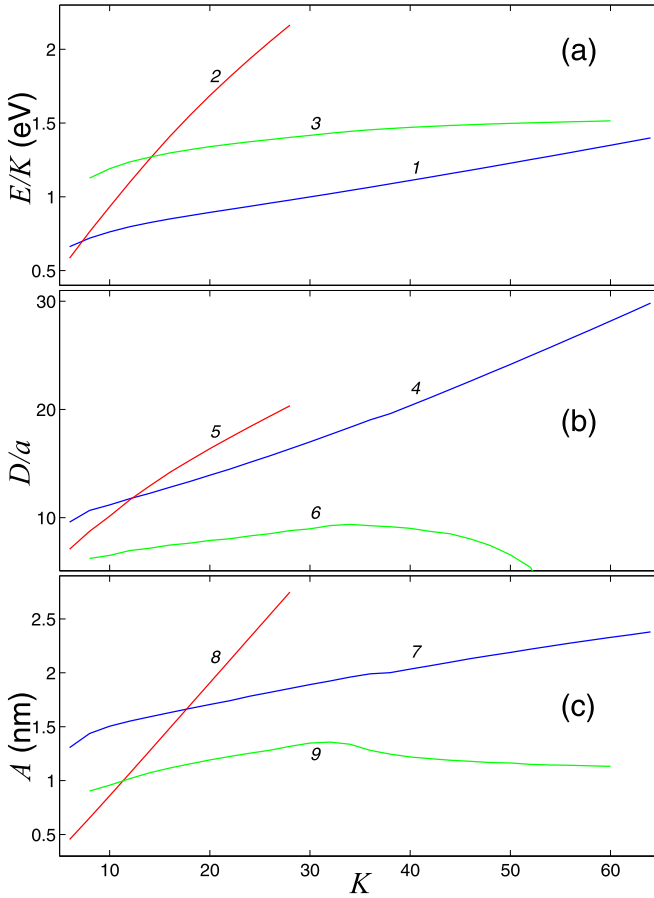


FIG. 7. Dependence of (a) energy, (b) width, and (c) amplitude on the nanoribbon width  $K$  for  $2\pi$  twiston (curves 1, 4, and 7),  $\pi$  twiston (curves 2, 5, and 8), and tilted fold (curves 3, 6, and 9). Potential energy in (a) is normalized to the nanoribbon width  $K$ ; width of the solitons  $D$  is normalized to the longitudinal period of the nanoribbon  $a$ .

larger  $K$ . The same is true for the amplitude of the considered topological solitons, as follows from (c).

#### IV. PROPERTIES OF MOVING TWISTONS

It turns out that  $\pi$  and  $2\pi$  twistons can move along the nanoribbon. Let us describe how twistons are set in motion in our calculations.

The Hamiltonian Eq. (1) defines the following set of equations of motion:

$$M \frac{d^2}{dt^2} \mathbf{u}_n = - \frac{\partial}{\partial \mathbf{u}_n} H, \quad n = 1, 2, \dots, N, \quad (23)$$

where  $\mathbf{u}_n = \{(x_{n,k}(t), y_{n,k}(t), z_{n,k}(t))\}_{k=1}^K$  is a  $3K$ -dimensional vector that defines atom coordinates of the  $n$ th transverse unit cell of the nanoribbon. Suppose that the set of equations of motion Eq. (23) has a solution in the form of a traveling solitary wave,

$$\mathbf{u}_n(t) = \mathbf{u}(na - st), \quad (24)$$

where  $a$  is the longitudinal period of the nanoribbon and  $s$  is the wave velocity. Then the second derivatives with respect to

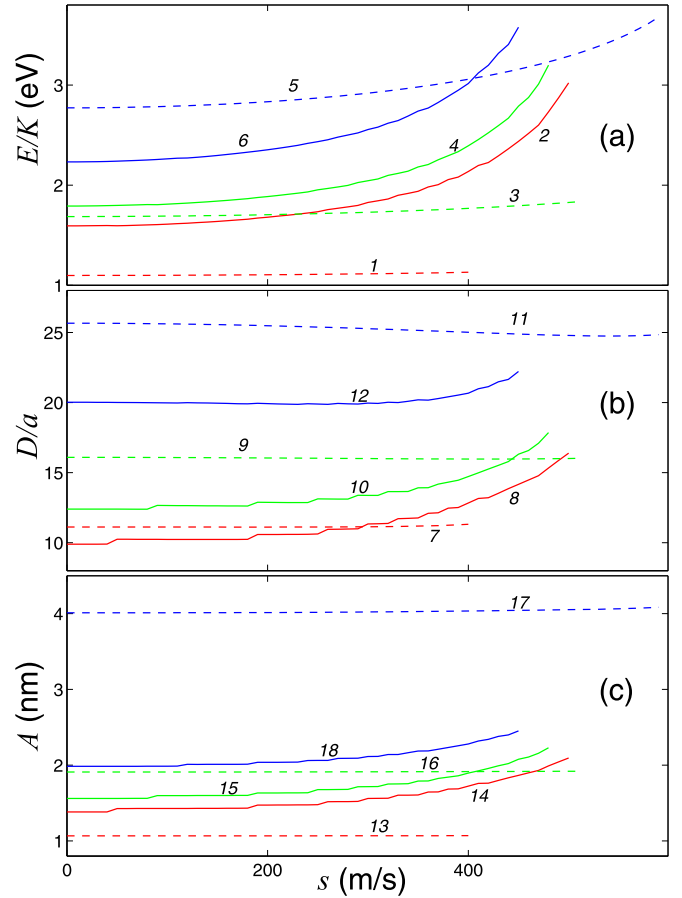


FIG. 8. Dependence of (a) energy, (b) width, and (c) amplitude on twiston velocity  $s$  for different nanoribbon widths  $K$ . Curves 1, 7, 13 and 2, 8, 14 give the dependencies for the  $\pi$  twiston and  $2\pi$  twiston, respectively, for the nanoribbon with  $K = 12$ . Curves 3, 9, 15 and 4, 10, 16 give the results for the  $\pi$  twiston and  $2\pi$  twiston, respectively, for the nanoribbon with  $K = 20$ . Curves 5, 11, 17 and 6, 12, 18 are for the  $\pi$  twiston and  $2\pi$  twiston, respectively, for  $K = 40$ .

time can be discretized as follows:

$$\frac{d^2}{dt^2} \mathbf{u}_n = s^2 (\mathbf{u}_{n+1} - 2\mathbf{u}_n + \mathbf{u}_{n-1}) / a^2. \quad (25)$$

Substituting Eq. (25) in the set of the equations of motion Eq. (23), one obtains a set of discrete equations whose solution is the extremal point of the functional

$$F = \sum_{n=1}^N \left\{ - \frac{Ms^2}{2a^2} \sum_{k=1}^K [(x_{n+1,k} - x_{n,k} - a)^2 + (y_{n+1,k} - y_{n,k})^2 + (z_{n+1,k} - z_{n,k})^2] + \frac{\partial}{\partial \mathbf{u}_n} (P + V + Z) \right\}. \quad (26)$$

Thus, a solitary wave in a nanoribbon can be sought as a solution to the minimization problem

$$F \rightarrow \min : \{\mathbf{u}_n\}_{n=1}^N. \quad (27)$$

The numerical solution of the minimization problem Eq. (27) has shown that solutions corresponding to  $\pi$  and  $2\pi$

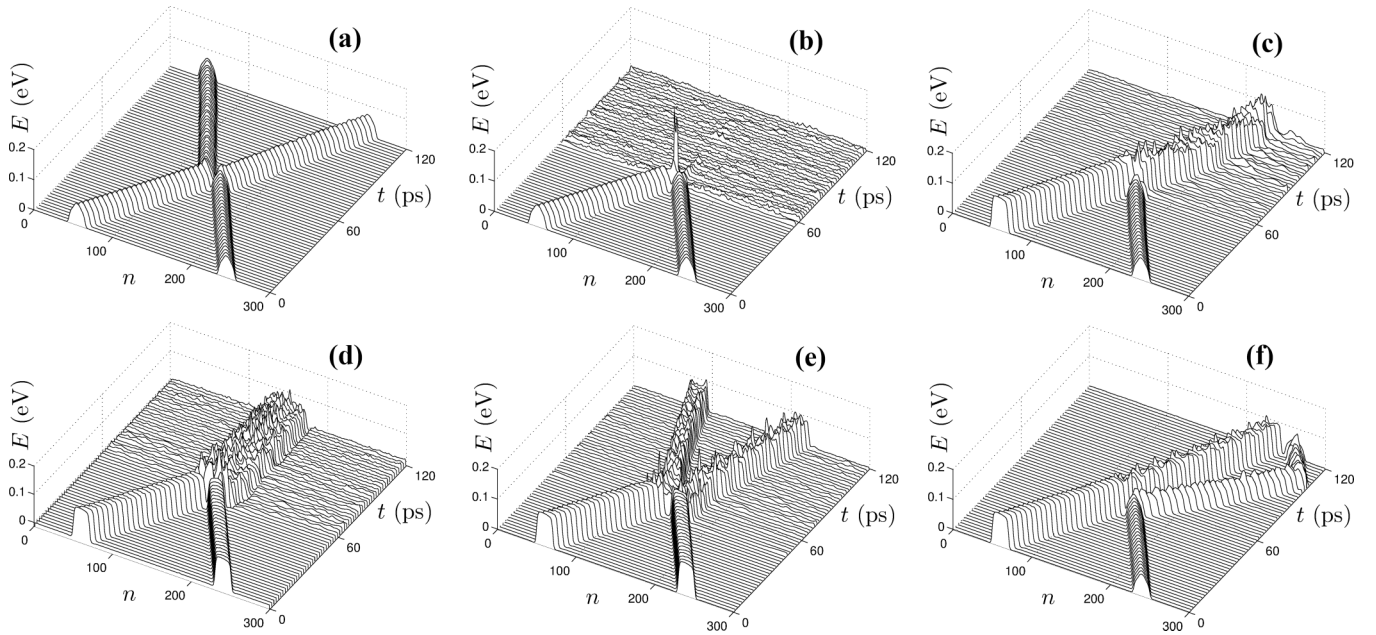


FIG. 9. Collision of (a) two  $\pi$  twistons, (b)  $\pi$  and  $-\pi$  twistons, (c)  $2\pi$  and  $\pi$  twistons, (d) two  $2\pi$  twistons, (e)  $2\pi$  and  $-2\pi$  twistons, and (f)  $2\pi$  and  $-\pi$  twistons. The time dependence of the energy distribution  $E$  along the nanoribbon is shown ( $n$  is the translational cell number). The nanoribbon consists of  $N = 300$  cells, in each cell  $K = 12$  atoms ( $L_x = 73.43$  nm,  $L_y = 1.134$  nm). The twistons have velocities  $s_1 = -s_2 = 400$  m/s =  $4 \text{ \AA}/\text{ps}$ .

twistons exist for velocities  $s \neq 0$ . If  $\{(x_{n,k}^0, y_{n,k}^0, z_{n,k}^0)_{k=1}^K\}_{n=1}^N$  is solution of the problem (27), then the solitary wave can be excited with the following initial conditions:

$$\begin{aligned} x_{n,k}(0) &= x_{n,k}^0, & y_{n,k}(0) &= y_{n,k}^0, & z_{n,k}(0) &= z_{n,k}^0, \\ \dot{x}_{n,k}(0) &= -s(x_{n+1,k}^0 - x_{n,k}^0 - a)/a, \\ \dot{y}_{n,k}(0) &= -s(y_{n+1,k}^0 - y_{n,k}^0)/a, \\ \dot{z}_{n,k}(0) &= -s(z_{n+1,k}^0 - z_{n,k}^0)/a. \end{aligned} \quad (28)$$

We note that the twistons can move only if the nanoribbon ends are parallel to each other. As can be seen from Figs. 3, 4, and 6, this condition is satisfied for  $\pi$  and  $2\pi$  twistons, but not always for  $4\pi$  twistons. This condition is also not met for the tilted fold shown in Fig. 3(d).

In Fig. 8, for moving  $\pi$  and  $2\pi$  twistons we show the dependencies of (a) twiston total energy, (b) width, and (c) amplitude on propagation velocity  $s$  for three different nanoribbon widths,  $K = 12, 20$ , and  $40$ . Curves 1, 7, 13 and 2, 8, 14 are for  $\pi$  and  $2\pi$  twistons, respectively, in the nanoribbon with  $K = 12$ ; curves 3, 9, 15 and 4, 10, 16 are for  $\pi$  and  $2\pi$  twistons, respectively, in the nanoribbon with  $K = 20$ ; curves 5, 11, 17 and 6, 12, 18 are for  $\pi$  and  $2\pi$  twistons, respectively, in the nanoribbon with  $K = 40$ .

Within the studied range of twiston velocities, they propagate along the nanoribbon as topological solitary waves that practically do not radiate energy. In particular, Figs. 9 and 10 show almost complete absence of radiation from traveling twistons before the collisions, and radiation can be seen after twiston collisions.

It can be seen from Fig. 8 that parameters of  $\pi$  twistons depend very weakly on twiston velocity (see dashed curves), especially in the narrow nanoribbon (curves 1, 7, 13 for  $K =$

12 and curves 3, 9, 15 for  $K = 20$ ). For the wider nanoribbon ( $K = 40$ ) the energy of the  $\pi$  twiston noticeably increases with velocity; see curve 5 in (a). For  $2\pi$  twistons all studied parameters noticeably increase with increasing  $s$ ; see solid curves in Fig. 8.

## V. TWISTON COLLISIONS

Since twistons can move as solitary waves practically radiating no energy (see Figs. 9–11); it is tempting to see the scenarios of twiston collisions.

Collisions will be called nearly elastic if the profile and velocities of twistons after the collision are nearly the same as those before the collision. If, as a result of a collision, the properties of twistons change noticeably, such collisions are considered inelastic.

Twiston collisions are simulated in the nanoribbon having  $N = 300$  transverse cells (length  $L_x = 73.43$  nm). At the initial time  $t = 0$ , the first twiston with a topological charge  $q_1$  and velocity  $s_1 = 400$  m/s is centered on the cell  $n_1 = 75$ . The second twiston with a topological charge  $q_2$  having a velocity  $s_2 = -s_1$  is centered on the cell  $n_2 = 225$ . The simulation was carried out in a nanoribbon with clamped edges  $n = 1$  and  $n = N$ . Collisions of twistons with charges  $q_1, q_2 = \pm\pi, \pm 2\pi$  in nanoribbons of width  $K = 12, 20, 40$  are shown in Figs. 9–11, respectively. Before the collision, the twistons move toward each other at a constant speed maintaining their profiles.

In a narrow nanoribbon with  $K = 12$ , the collision of  $\pi$  twistons ( $q_1 = q_2 = \pi$ ) occurs almost elastically; the twistons are reflected from each other [see Fig. 9(a)]. Collision of twistons of the opposite sign ( $q_1 = \pi, q_2 = -\pi$ ) leads to their recombination [see Fig. 9(b)]. The collision of  $2\pi$  twistons ( $q_1 = q_2 = 2\pi$ ) leads to the formation of their bound state



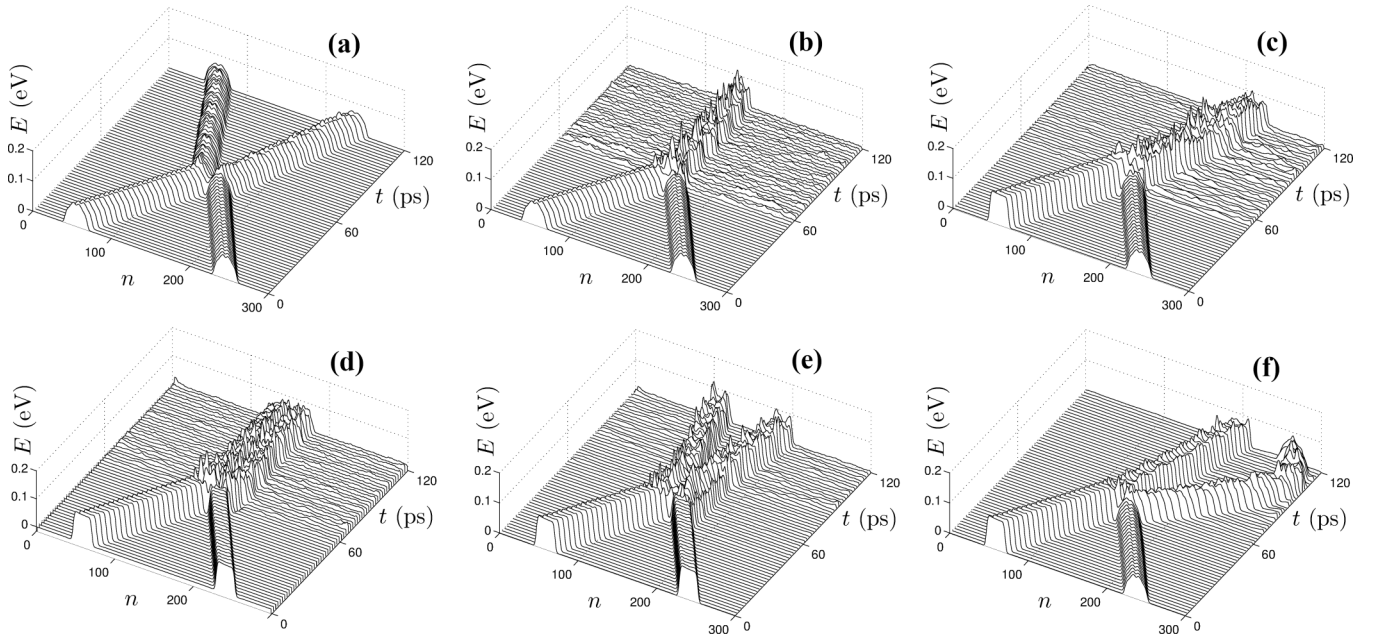


FIG. 10. Collision of (a) two  $\pi$  twistons, (b)  $\pi$  and  $-\pi$  twistons, (c)  $2\pi$  and  $\pi$  twistons, (d) two  $2\pi$  twistons, (e)  $2\pi$  and  $-2\pi$  twistons, and (f)  $2\pi$  and  $-\pi$  twistons. The time dependence of the energy distribution  $E$  along the nanoribbon is shown ( $n$  is the translational cell number). The nanoribbon consists of  $N = 300$  cells, in each cell  $K = 20$  atoms ( $L_x = 73.43$  nm,  $L_y = 1.985$  nm). The velocity of twistons is  $s_1 = -s_2 = 400$  m/s =  $4 \text{ \AA/ps}$ .

[stationary  $4\pi$  twiston; see Fig. 9(d)]. Collision of  $2\pi$  twistons of the opposite signs ( $q_1 = 2\pi$ ,  $q_2 = -2\pi$ ) leads to their inelastic reflection accompanied by intense phonon emission [see Fig. 9(e)]. For twistons with topological charges  $q_1 = 2\pi$ ,  $q_2 = \pi$  a collision leads to the formation of their bound state, accompanied by intense energy release [see Fig. 9(c)].

For  $q_1 = 2\pi$ ,  $q_2 = -\pi$  the collision of the twistons leads to their inelastic reflection [see Fig. 9(f)].

An increase in the width of the nanoribbon does not lead to a qualitative change in the collision scenarios, only the inelasticity of collisions is enhanced. So in a nanoribbon with  $K = 20$  and  $40$ , the collision of twistons with

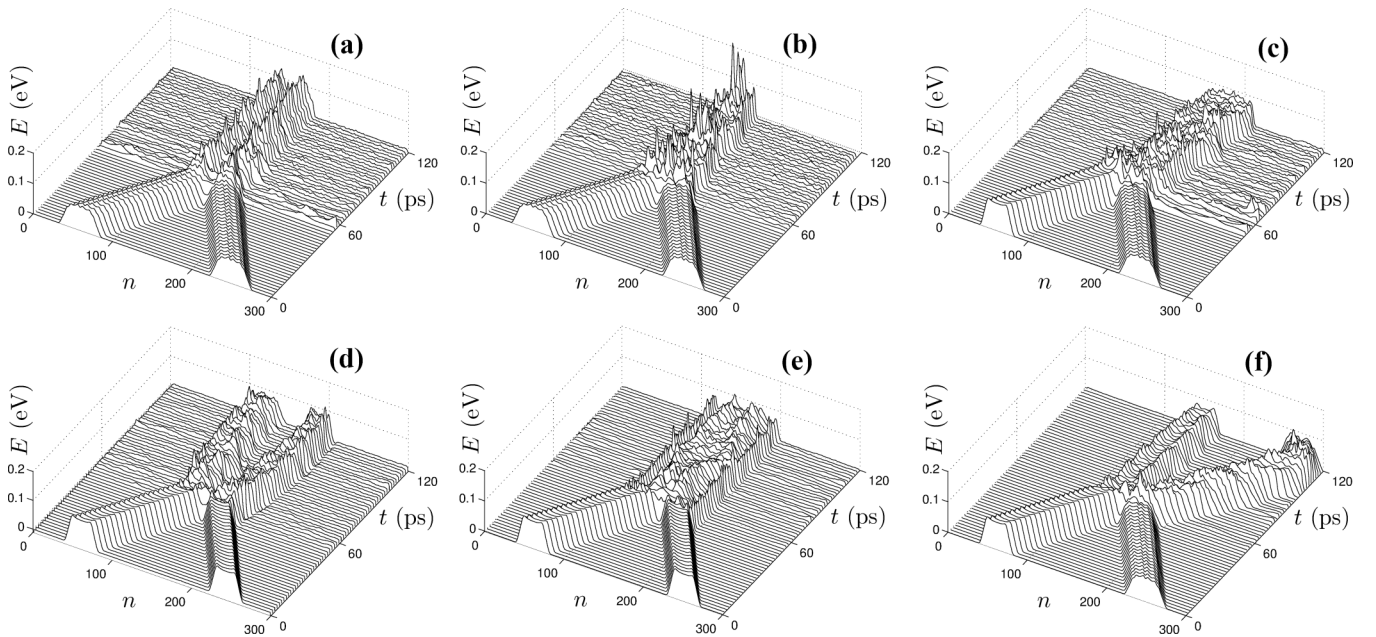


FIG. 11. Collision of (a) two  $\pi$  twistons, (b)  $\pi$  and  $-\pi$  twistons, (c)  $2\pi$  and  $\pi$  twistons, (d) two  $2\pi$  twistons, (e)  $2\pi$  and  $-2\pi$  twistons, and (f)  $2\pi$  and  $-\pi$  twistons. The time dependence of the energy distribution  $E$  along the nanoribbon is shown ( $n$  is the translational cell number). The nanoribbon consists of  $N = 300$  cells, in each cell  $K = 40$  atoms ( $L_x = 73.43$  nm,  $L_y = 4.112$  nm). The velocity of twistons is  $s_1 = -s_2 = 400$  m/s =  $4 \text{ \AA/ps}$ .



topological charges  $q_1 = \pi$ ,  $q_2 = -\pi$  leads to the formation of a fold (ripplocation [68]) having a zero topological charge [see Fig. 10(b) and Fig. 11(b)]. In a nanoribbon with  $K = 40$ , the collision of twistons with the same charges  $q_1 = q_2 = \pi$  already leads not to their repulsion, but to the formation of a stationary bound state with a topological charge  $q = 2\pi$  [see Fig. 11(a)]. Collision of  $2\pi$  twistons of the same sign already leads to their inelastic reflection from each other [see Fig. 11(d)], and the collision of  $2\pi$  twistons of the opposite sign results in the formation of a stationary vertical fold [see Fig. 11(e)].

## VI. CONCLUSIONS

Using molecular dynamics simulations, it was shown that the spatial localization of twisting in a twisted nanoribbon occurs due to interaction with the substrate. Localized twisted regions behave like topological solitons, called twistons here. Energy, width, and amplitude of static  $\pi$  and  $2\pi$  twistons were determined as the functions of nanoribbon width; see Fig. 7.

It was demonstrated that twistons can be set in motion; see Sec. IV. For the velocities less than  $4 \text{ \AA}/\text{ps}$ ,  $\pi$  and  $2\pi$  twistons propagate practically radiating no energy. Energy, width, and amplitude of moving  $\pi$  and  $2\pi$  twistons were determined as the functions of propagation velocity for different values of nanoribbon width; see Fig. 8. Parameters of  $\pi$  twistons

depend very weakly on the velocity, while for  $2\pi$  twistons the effect of propagation velocity on twistons' properties is more pronounced.

Collisions of twistons with various positive and negative topological charges were analyzed. In narrow nanoribbons, collisions are more elastic and more reminiscent of collisions of topological solitons in Klein-Gordon systems [83–88]. In particular, in narrow nanoribbons,  $\pi$  twistons of the same charge repel each other like Klein-Gordon kinks, while they attract each other and annihilate in the case of opposite charge, like a Klein-Gordon kink and antikink. In wider nanoribbons collisions are less elastic and twistons of the same and opposite charge tend to form bound states, which is unusual for the Klein-Gordon solitary waves.

Static and dynamic properties of twistons and their collisions reported here for graphene nanoribbon on graphite substrate can be similar to those for nanoribbons and substrates of different chemical composition.

## ACKNOWLEDGMENTS

A.V.S. acknowledges financial support from the Russian Foundation for Basic Research, Grant No. 18-29-19135. The work was partly supported by the State Assignment of IMSP RAS No. AAAA-A17-117041310220-8. The research was carried out using supercomputers at the Joint Supercomputer Center of the Russian Academy of Sciences (JSCC RAS).

- 
- [1] S. Berber, Y.-K. Kwon, and D. Tománek, *Phys. Rev. Lett.* **84**, 4613 (2000).
  - [2] A. A. Balandin, S. Ghosh, W. Bao, I. Calizo, D. Teweldebrhan, F. Miao, and C. N. Lau, *Nano Lett.* **8**, 902 (2008).
  - [3] C. Lee, X. Wei, J. W. Kysar, and J. Hone, *Science* **321**, 385 (2008).
  - [4] M.-F. Yu, O. Lourie, M. J. Dyer, K. Moloni, T. F. Kelly, and R. S. Ruoff, *Science* **287**, 637 (2000).
  - [5] A. B. Kuzmenko, E. van Heumen, F. Carbone, and D. van der Marel, *Phys. Rev. Lett.* **100**, 117401 (2008).
  - [6] A. K. Geim and K. S. Novoselov, *Nat. Mater.* **6**, 183 (2007).
  - [7] A. Fabbro, D. Scaini, V. Leon, E. Vazquez, G. Cellot, G. Privitera, L. Lombardi, F. Torrisi, F. Tomarchio, F. Bonaccorso *et al.*, *ACS Nano* **10**, 615 (2016).
  - [8] N. Yang, X. Ni, J.-W. Jiang, and B. Li, *Appl. Phys. Lett.* **100**, 093107 (2012).
  - [9] A. V. Savin, E. A. Korznikova, and S. V. Dmitriev, *Phys. Solid State* **57**, 2348 (2015).
  - [10] B. Jayasena, S. Subbiah, and C. D. Reddy, *J. Micro Nano-Manuf.* **2**, 011003 (2014).
  - [11] A. V. Savin, E. A. Korznikova, and S. V. Dmitriev, *Phys. Rev. B* **92**, 035412 (2015).
  - [12] T. Uhm, J. Na, J.-U. Lee, H. Cheong, S. Lee, E. Campbell, and S. Jhang, *Nanotechnology* **31**, 315707 (2020).
  - [13] A. Savin, E. Korznikova, S. Dmitriev, and E. Soboleva, *Comput. Mater. Sci.* **135**, 99 (2017).
  - [14] Q. Yin and X. Shi, *Nanoscale* **5**, 5450 (2013).
  - [15] S. Deng and V. Berry, *Mater. Today* **19**, 197 (2016).
  - [16] E. A. Korznikova and S. V. Dmitriev, *J. Phys. D: Appl. Phys.* **47**, 345307 (2014).
  - [17] G. Anagnostopoulos, G. Paterakis, I. Polyzos, P.-N. Pappas, K. Kouroupis-Agalou, N. Mirotta, A. Scida, V. Palermo, J. Parthenios, K. Papagelis *et al.*, *ACS Appl. Mater. Interfaces* **10**, 43192 (2018).
  - [18] J. Baimova, S. Dmitriev, and K. Zhou, *Phys. Status Solidi B* **249**, 1393 (2012).
  - [19] J. Zang, S. Ryu, N. Pugno, Q. Wang, Q. Tu, M. J. Buehler, and X. Zhao, *Nat. Mater.* **12**, 321 (2013).
  - [20] J. A. Baimova, E. A. Korznikova, S. V. Dmitriev, B. Liu, and K. Zhou, *Rev. Adv. Mater. Sci.* **39**, 69 (2014).
  - [21] X. Ning, X. Wang, Y. Zhang, X. Yu, D. Choi, N. Zheng, D. Kim, Y. Huang, Y. Zhang, and J. Rogers, *Adv. Mater. Interfaces* **5**, 1800284 (2018).
  - [22] P.-Y. Chen, M. Liu, Z. Wang, R. Hurt, and I. Wong, *Adv. Mater.* **29**, 1605096 (2017).
  - [23] Y. Zhang, F. Zhang, Z. Yan, Q. Ma, X. Li, Y. Huang, and J. Rogers, *Nat. Rev. Mater.* **2**, 17019 (2017).
  - [24] M. Blees, A. Barnard, P. Rose, S. Roberts, K. McGill, P. Huang, A. Ruyack, J. Kevek, B. Kobrin, D. Muller *et al.*, *Nature (London)* **524**, 204 (2015).
  - [25] L. Dong, C. Xu, Y. Li, C. Wu, B. Jiang, Q. Yang, E. Zhou, F. Kang, and Q.-H. Yang, *Adv. Mater.* **28**, 1675 (2016).
  - [26] L. K. Rysaeva, E. A. Korznikova, R. T. Murzaev, D. U. Abdullina, A. A. Kudreyko, J. A. Baimova, D. S. Lisovenko, and S. V. Dmitriev, *Facta Univ., Ser.: Mech. Eng.* **18**, 1 (2020).
  - [27] D. Abdullina, E. Korznikova, V. Dubinko, D. Laptev, A. Kudreyko, E. Soboleva, S. Dmitriev, and K. Zhou, *Computation* **8**, 27 (2020).
  - [28] E. Korznikova, L. Rysaeva, A. Savin, E. Soboleva, E. Ekomasov, M. Ilgamov, and S. Dmitriev, *Materials* **12**, 3951 (2019).

- [29] Z. Y. Rong and P. Kuiper, *Phys. Rev. B* **48**, 17427 (1993).
- [30] J. Hass, F. Varchon, J. E. Millan-Otoya, M. Sprinkle, N. Sharma, W. A. de Heer, C. Berger, P. N. First, L. Magaud, and E. H. Conrad, *Phys. Rev. Lett.* **100**, 125504 (2008).
- [31] A. Luican, G. Li, A. Reina, J. Kong, R. R. Nair, K. S. Novoselov, A. K. Geim, and E. Y. Andrei, *Phys. Rev. Lett.* **106**, 126802 (2011).
- [32] O. O. Kit, T. Tallinen, L. Mahadevan, J. Timonen, and P. Koskinen, *Phys. Rev. B* **85**, 085428 (2012).
- [33] K. V. Bets and B. I. Yakobson, *Nano Res.* **2**, 161 (2009).
- [34] E. Moraes Diniz, *Appl. Phys. Lett.* **104**, 083119 (2014).
- [35] D. Xia, Q. Li, Q. Xue, C. Liang, and M. Dong, *Phys. Chem. Chem. Phys.* **18**, 18406 (2016).
- [36] A. V. Savin and Y. S. Kivshar, *Phys. Rev. B* **96**, 064307 (2017).
- [37] Y. Huang, Y. Mai, X. Yang, U. Beser, J. Liu, F. Zhang, D. Yan, K. Müllen, and X. Feng, *J. Am. Chem. Soc.* **137**, 11602 (2015).
- [38] H. Vandeparre, M. Pineirua, F. Brau, B. Roman, J. Bico, C. Gay, W. Bao, C. N. Lau, P. M. Reis, and P. Damman, *Phys. Rev. Lett.* **106**, 224301 (2011).
- [39] Z. Chen, G. Huang, I. Trase, X. Han, and Y. Mei, *Phys. Rev. Appl.* **5**, 017001 (2016).
- [40] A. Awasthi, S. Bhagat, R. Ramakrishnan, and A. Srivastava, *Chem. - Eur. J.* **25**, 12905 (2019).
- [41] G. Zaldivar, M. Conda-Sheridan, and M. Tagliazucchi, *J. Phys. Chem. B* **124**, 3221 (2020).
- [42] S. Bae, H. Kim, Y. Lee, X. Xu, J.-S. Park, Y. Zheng, J. Balakrishnan, T. Lei, H. Ri Kim, Y. Song *et al.*, *Nat. Nanotechnol.* **5**, 574 (2010).
- [43] G. Fiori, F. Bonaccorso, G. Iannaccone, T. Palacios, D. Neumaier, A. Seabaugh, S. Banerjee, and L. Colombo, *Nat. Nanotechnol.* **9**, 768 (2014).
- [44] Y. Liu, N. Weiss, X. Duan, H.-C. Cheng, Y. Huang, and X. Duan, *Nat. Rev. Mater.* **1**, 16042 (2016).
- [45] U. Moger and G. U. Kulkarni, *Carbon* **156**, 470 (2020).
- [46] Y. Li, *J. Phys. D: Appl. Phys.* **43**, 495405 (2010).
- [47] A. Savin, E. Korznikova, and S. Dmitriev, *Mech. Mater.* **137**, 103123 (2019).
- [48] A. Savin, E. Korznikova, A. Krivtsov, and S. Dmitriev, *Eur. J. Mech. A: Solids* **80**, 103920 (2020).
- [49] T.-H. Fang, W.-J. Chang, Y.-L. Feng, and D.-M. Lu, *Physica E* **83**, 263 (2016).
- [50] H. Zhan, G. Zhang, C. Yang, and Y. Gu, *Nanoscale* **10**, 18961 (2018).
- [51] A. Sadrzadeh, M. Hua, and B. Yakobson, *Appl. Phys. Lett.* **99**, 013102 (2011).
- [52] T. Ma, S. Wen, C. Wu, L. Yan, M. Zhang, Y. Kan, and Z. Su, *J. Mater. Chem. C* **3**, 10085 (2015).
- [53] N. Xu, B. Huang, J. Li, and B. Wang, *Solid State Commun.* **202**, 39 (2015).
- [54] M. Watanabe, H. Komatsu, N. Tsuji, and H. Aoki, *Phys. Rev. B* **92**, 205425 (2015).
- [55] V. Atanasov and A. Saxena, *Phys. Rev. B* **92**, 035440 (2015).
- [56] S. Carmel, S. Subramanian, R. Rathinam, and A. Bhattacharyya, *J. Appl. Phys.* **127**, 094303 (2020).
- [57] M. Saiz-Bretin, F. Dominguez-Adame, and A. Malyshev, *Carbon* **149**, 587 (2019).
- [58] R. Thakur, P. Ahluwalia, A. Kumar, B. Mohan, and R. Sharma, *Physica E* **124**, 114280 (2020).
- [59] N. Wei, L. Xu, H.-Q. Wang, and J.-C. Zheng, *Nanotechnology* **22**, 105705 (2011).
- [60] R. Chellattoan and S. P. Sathian, *Solid State Commun.* **173**, 1 (2013).
- [61] H. Shen, *Mol. Phys.* **112**, 2614 (2014).
- [62] X. Wei, G. Guo, T. Ouyang, and H. Xiao, *J. Appl. Phys.* **115**, 154313 (2014).
- [63] S. Chen, Q. Li, Q. Zhang, Y. Qu, H. Ji, R. S. Ruoff, and W. Cai, *Nanotechnology* **23**, 365701 (2012).
- [64] J. Zhao, J. Wu, J.-W. Jiang, L. Lu, Z. Zhang, and T. Rabczuk, *Appl. Phys. Lett.* **103**, 233511 (2013).
- [65] A. Antidormi, M. Royo, and R. Rurali, *J. Phys. D: Appl. Phys.* **50**, 234005 (2017).
- [66] B. Mortazavi, A. Lherbier, Z. Fan, A. Harju, T. Rabczuk, and J.-C. Charlier, *Nanoscale* **9**, 16329 (2017).
- [67] I. Shepelev, A. Chetverikov, S. Dmitriev, and E. Korznikova, *Comput. Mater. Sci.* **177**, 109549 (2020).
- [68] A. V. Savin, E. A. Korznikova, and S. V. Dmitriev, *Phys. Rev. B* **99**, 235411 (2019).
- [69] M. Barsoum, *Front. Mater.* **7**, 146 (2020).
- [70] A. Kushima, X. Qian, P. Zhao, S. Zhang, and J. Li, *Nano Lett.* **15**, 1302 (2015).
- [71] A. Ostadhosseini, A. Rahnamoun, Y. Wang, P. Zhao, S. Zhang, V. Crespi, and A. Van Duin, *J. Phys. Chem. Lett.* **8**, 631 (2017).
- [72] A. Alaferdov, R. Savu, M. Canesqui, Y. Kopelevich, R. da Silva, N. Rozhkova, D. Pavlov, Y. Usov, G. de Trindade, and S. Moshkalev, *Carbon* **129**, 826 (2018).
- [73] I. Evazzade, I. P. Lobzenko, E. A. Korznikova, I. A. Ovid'Ko, M. R. Roknabadi, and S. V. Dmitriev, *Phys. Rev. B* **95**, 035423 (2017).
- [74] E. Barani, E. A. Korznikova, A. P. Chetverikov, K. Zhou, and S. V. Dmitriev, *Phys. Lett. A* **381**, 3553 (2017).
- [75] E. Barani, I. Lobzenko, E. Korznikova, E. Soboleva, S. Dmitriev, K. Zhou, and A. Marjaneh, *Eur. Phys. J. B* **90**, 38 (2017).
- [76] D. Sanchez-Portal, E. Artacho, J. M. Soler, A. Rubio, and P. Ordejon, *Phys. Rev. B* **59**, 12678 (1999).
- [77] C. L. Kane and E. J. Mele, *Phys. Rev. Lett.* **78**, 1932 (1997).
- [78] A. V. Savin, Y. S. Kivshar, and B. Hu, *Phys. Rev. B* **82**, 195422 (2010).
- [79] D. W. Noid, B. G. Sumpter, and B. Wunderlich, *Macromolecules* **24**, 4148 (1991).
- [80] R. Setton, *Carbon* **34**, 69 (1996).
- [81] A. Savin and O. Savina, *Phys. Solid State* **61**, 2241 (2019).
- [82] A. V. Savin and Y. S. Kivshar, *Europhys. Lett.* **82**, 66002 (2008).
- [83] H. Yan, Y. Zhong, Y.-X. Liu, and K.-I. Maeda, *Phys. Lett. B* **807**, 135542 (2020).
- [84] Y. Zhong, X.-L. Du, Z.-C. Jiang, Y.-X. Liu, and Y.-Q. Wang, *J. High Energy Phys.* **02** (2020) 153.
- [85] A. Askari, A. Moradi Marjaneh, Z. Rakhmatullina, M. Ebrahimi-Loushab, D. Saadatmand, V. Gani, P. Kevrekidis, and S. Dmitriev, *Chaos, Solitons Fractals* **138**, 109854 (2020).
- [86] E. Belendryasova and V. Gani, *Commun. Nonlinear Sci. Numer. Simul.* **67**, 414 (2019).
- [87] S. V. Dmitriev, P. G. Kevrekidis, and Y. S. Kivshar, *Phys. Rev. E* **78**, 046604 (2008).
- [88] S. V. Dmitriev, Y. S. Kivshar, and T. Shigenari, *Phys. Rev. E* **64**, 056613 (2001).